Possible coexistence of magnetic and antimagnetic rotations in ^{61}Ni

J. Lin,[1] Y. K. Wang,[1] C. Xu,[1,*] Z. H. Li,[1,†] H. Hua,[1,‡] S. Q. Zhang,[1] D. W. Luo,[1] H. Y. Wu,[1] J. Meng,[1] X. G. Wu,[2] Y. Zheng,[2] C. B. Li,[2] T. X. Li,[2] Z. Y. Huang,[2] H. Cheng,[2] C. Y. Guo,[2] Z. X. Zhou,[2] Z. Q. Chen,[2] and C. G. Wang[2]
[1]*School of Physics and State Key Laboratory of Nuclear Physics and Technology, Peking University, Beijing 100871, China*
[2]*China Institute of Atomic Energy, Beijing 102413, China*

(Received 10 October 2022; accepted 4 January 2023; published 17 January 2023)

The high-spin spectroscopy of ^{61}Ni has been studied by the fusion-evaporation reaction ^{54}Cr(^{11}B, $4n$)^{61}Ni at a beam energy of 54 MeV. One dipole band and one quadrupole band in ^{61}Ni are established for the first time. They can be respectively taken as candidates of magnetic and antimagnetic rotational bands based on the comparison with the well-known cases in ^{110}Cd and the calculations of the classical particles-plus-rotor model. These two new bands are further investigated by the microscopic tilted axis cranking covariant density functional theory with configurations $\pi[(1f_{7/2})^{-1}(fp)^1] \otimes \nu[(1g_{9/2})^1(fp)^4]$ and $\pi[(1f_{7/2})^{-2}(fp)^2] \otimes \nu[(1g_{9/2})^1(fp)^4]$, respectively, and good agreement between experiment and calculation is obtained. By examining the angular-momentum coupling, the dipole band is characterized by the shears mechanism whereas the quadrupole band is characterized by the two-shears-like mechanism. This study provides evidence for possible coexistence of magnetic and antimagnetic rotations in the $A \approx 60$ mass region.

DOI: 10.1103/PhysRevC.107.014307

I. INTRODUCTION

Magnetic rotational (MR) bands in almost spherical or weakly deformed nuclei, which were interpreted in terms of the shears mechanism [1,2], have attracted great interest in the past two decades [3–6]. In these bands, the magnetic-dipole vector, which arises from proton particles (holes) and neutron holes (particles) in high-j orbitals, rotates around the total angular-momentum vector. At the bandhead, the proton and neutron angular momenta are almost perpendicular to each other. With the increase of the rotational frequency, the energy and angular momentum are increased mainly by the gradual alignments of the proton and neutron angular momenta along the total angular momentum, and consequently the orientation of the total angular momentum in the intrinsic frame does not change much [7].

As another mechanism to generate the rotational bands in almost spherical or weakly deformed nuclei, the antimagnetic rotation (AMR) [4,8] is characterized by the so-called "two-shears-like mechanism". Two blades of valence protons (neutrons) are aligned back to back in opposite directions and nearly perpendicular to the total angular momentum of the valence neutrons (protons) at the bandhead, which together constitute two pairs of shears. With the increase of the rotational frequency, the energy and angular momentum are increased by the simultaneous closings of the two pairs of shears. In contrast with the strong magnetic-dipole ($M1$) transitions in MR bands, the two magnetic-dipole vectors arising from the two pairs of shears cancel each other in AMR due to the symmetry of the structure. Thus, the $M1$ transitions vanish and the energy levels in AMR bands are connected by weak electric-quadrupole ($E2$) transitions reflecting small deformations of nuclei.

To date, hundreds of MR bands have been reported over a wide range of mass number, most around the $A \approx 80$, 110, 140, and 190 mass regions [3–6]. Compared with the well-established MR phenomenon, the experimental evidence on AMR is relatively scarce. The AMR bands have been observed only in the $A \approx 110$ and 140 mass regions, particularly in Ru [9], Pd [10–15], Cd [16–22], In [23–26], Nd [27], Eu [28,29], and Dy [30] isotopes. Since both of AMR and MR are the manifestations of the shears mechanism and associated with the high-j proton and neutron orbitals near the Fermi surface, AMR is expected to occur in the same mass region, even in the same nucleus, as MR [31]. Therefore, it is interesting to search for the candidates of AMR bands outside the $A \approx 110$, 140 mass regions and to investigate the coexistence of AMR and MR bands in one single nucleus.

Atomic nuclei in the $A \approx 60$ mass region lying close to the $Z = 28$ shell closure contain one or more proton holes in the $f_{7/2}$ orbitals and valence neutrons in the $f_{5/2}$ and $g_{9/2}$ orbitals in their ground and excited states. These nuclei are suitable for searching the AMR and MR structures. Indeed, MR bands have been reported in ^{58}Fe [32] and ^{60}Ni [33], which mark the lightest mass region of MR observed so far. In this article, we report the heavy-ion fusion-evaporation reaction study for ^{61}Ni. The structure of ^{61}Ni has been studied in a variety of experiments [34] including the heavy-ion fusion-evaporation reactions [35–38], but no obvious collective structures were reported. In the present work, the collective structures especially a dipole band and a quadrupole band in ^{61}Ni are

*chuan@pku.edu.cn
†zhli@pku.edu.cn
‡hhua@pku.edu.cn

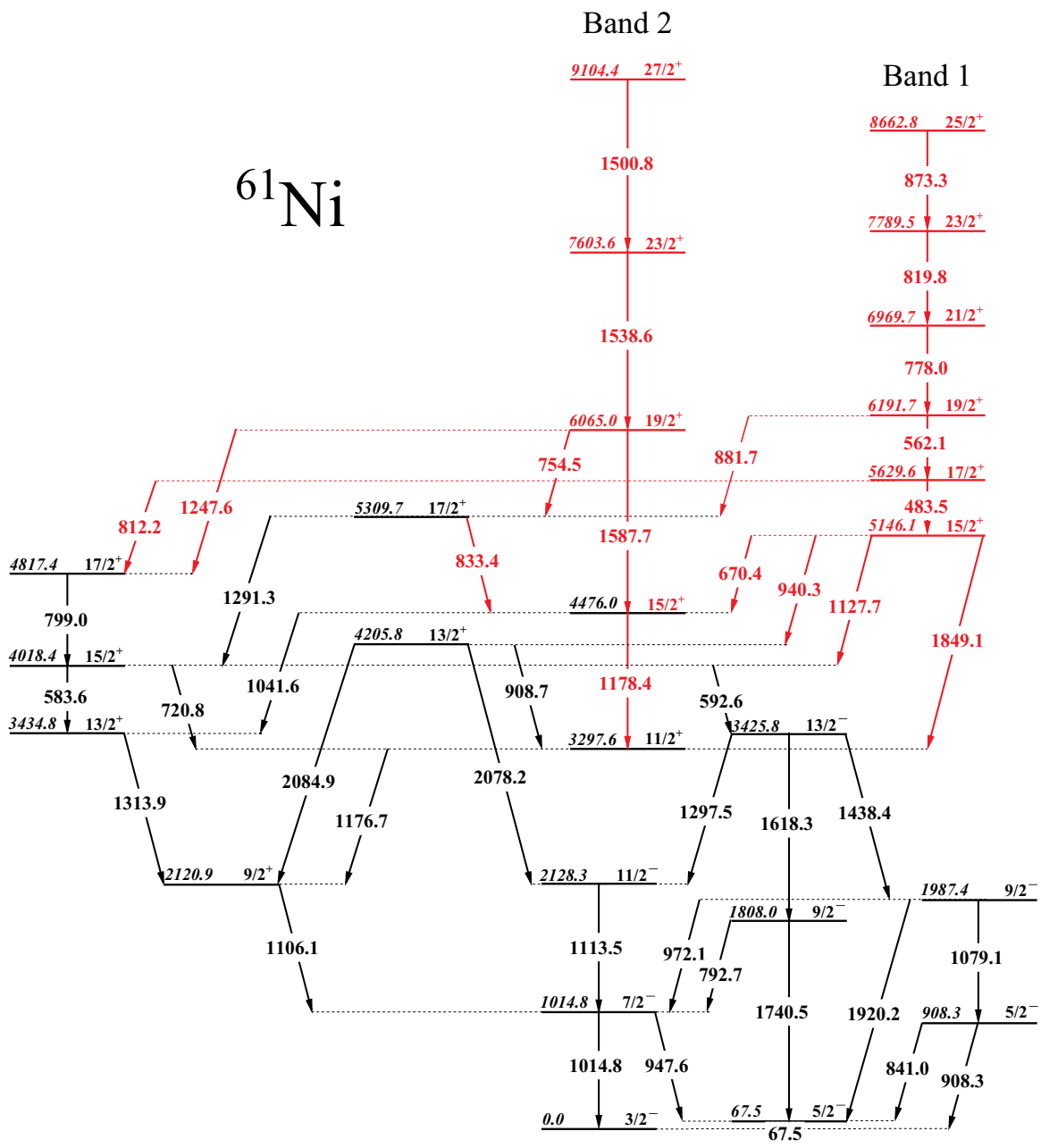

FIG. 1. Partial level scheme of ^{61}Ni. Energies are given in keV. New transitions and levels are marked as red.

established for the first time. These two bands can be interpreted as the coexistence of MR and AMR bands by analyzing the angular-momentum-forming mechanism with the microscopic tilted axis cranking covariant density functional theory (TAC-CDFT).

II. EXPERIMENT

The experiment was performed at the HI-13 tandem facility of the China Institute of Atomic Energy (CIAE). High-spin states of ^{61}Ni were populated via the fusion-evaporation reaction ^{54}Cr(^{11}B, 4n)^{61}Ni at a beam energy of 54 MeV. The ^{54}Cr target with a thickness of 1.0 mg/cm^2 on 8.9 mg/cm^2 Au backing was used. The in-beam γ rays were detected by a detector array which consists of six high-purity germanium (HPGe) with bismuth germinate (BGO) anti-Compton suppressors, one clover HPGe detector, and two planar HPGe detectors. Standard ^{152}Eu and ^{133}Ba γ-ray sources were used to calibrate all detectors.

A total of 2.33×10^8 γ-γ coincident events were collected from which a symmetric matrix was built. The level scheme analysis was performed by using the RADWARE software [39]. To determine the multipolarities of the γ-ray transitions, two asymmetric angular distributions from oriented states (ADO) [40] matrices were constructed by using the γ rays detected at all angles (the y axis) against those detected at 90° and 40° (the x axis), respectively. The multipolarities of the emitted γ rays were analyzed by means of the ADO ratio, defined

TABLE I. γ-ray energies, excitation energies, relative γ-ray intensities, and ADO ratios in ^{61}Ni.

E_γ (keV)[a]	E_i (keV)	E_f (keV)	Relative intensity	ADO ratio	Assignment
66.7	66.7	0.0			$5/2^- \rightarrow 3/2^-$
483.5	5629.6	5146.1	16.3(17)	0.77(10)	$17/2^+ \rightarrow 15/2^+$
562.1	6191.7	5629.6	12.9(16)	0.87(10)	$19/2^+ \rightarrow 17/2^+$
583.6	4018.4	3434.8	8.9(10)	1.54(19)	$15/2^+ \rightarrow 13/2^+$
592.6	4018.4	3425.8	30.5(19)	0.97(11)	$15/2^+ \rightarrow 13/2^-$
670.4	5146.1	4476.0	2.9(3)	1.52(25)	$15/2^+ \rightarrow 15/2^+$
720.8	4018.4	3297.6	7.4(8)	1.86(23)	$15/2^+ \rightarrow 11/2^+$
754.5	6065.0	5309.7	2.3(3)	1.20(17)	$19/2^+ \rightarrow 17/2^+$
778.0	6969.7	6191.7	8.5(9)	1.11(13)	$21/2^+ \rightarrow 19/2^+$
792.7	1807.5	1014.8	3.0(4)	1.08(17)	$9/2^- \rightarrow 7/2^-$
799.0	4817.4	4018.4	12.3(16)	0.90(8)	$17/2^+ \rightarrow 15/2^+$
812.2	5629.6	4817.4	3.6(6)	1.15(14)	$17/2^+ \rightarrow 17/2^+$
819.8	7789.5	6969.7	5.8(2)	0.78(12)	$23/2^+ \rightarrow 21/2^+$
833.4	5309.7	4476.0	3.5(12)	1.20(22)	$17/2^+ \rightarrow 15/2^+$
841.0	908.3	66.7	19.5(12)	1.48(21)	$5/2^- \rightarrow 5/2^-$
873.3	8662.8	7789.5	4.1(3)	0.70(15)	$25/2^+ \rightarrow 23/2^+$
880.7	6191.7	5309.7	9.6(14)	1.62(19)	$19/2^+ \rightarrow 17/2^+$
908.3	908.3	0.0	13.4(13)	1.05(11)	$5/2^- \rightarrow 3/2^-$
908.7	4205.8	3297.6	3.4(3)	1.53(26)	$13/2^+ \rightarrow 11/2^+$
940.3	5146.1	4205.8	9.1(7)	0.88(12)	$15/2^+ \rightarrow 13/2^+$
947.6	1014.8	66.7	100	1.77(14)	$7/2^- \rightarrow 5/2^-$
972.1	1987.4	1014.8	5.4(4)	0.86(12)	$9/2^- \rightarrow 7/2^-$
1014.8	1014.8	0.0	52.9(11)	1.85(17)	$7/2^- \rightarrow 3/2^-$
1041.6	4476.0	3434.8	13.0(13)	1.32(14)	$15/2^+ \rightarrow 13/2^+$
1079.1	1987.4	908.3	15.4(3)	1.92(20)	$9/2^- \rightarrow 5/2^-$
1106.1	2120.9	1014.8	72.5(21)	0.95(8)	$9/2^+ \rightarrow 7/2^-$
1113.5	2128.3	1014.8	32.4(22)	1.29(12)	$11/2^- \rightarrow 7/2^-$
1127.7	5146.1	4018.4	2.7(4)	1.32(19)	$15/2^+ \rightarrow 15/2^+$
1176.7	3297.6	2120.9	16.3(16)[b]		$11/2^+ \rightarrow 9/2^+$
1178.4	4476.0	3297.6	16.3(16)[b]		$15/2^+ \rightarrow 11/2^+$
1247.6	6065.0	4817.4	3.2(5)	1.28(19)	$19/2^+ \rightarrow 17/2^+$
1291.3	5309.7	4018.4	8.8(14)	1.06(10)	$17/2^+ \rightarrow 15/2^+$
1297.5	3425.8	2128.3	11.2(9)	1.05(10)	$13/2^- \rightarrow 11/2^-$
1313.9	3434.8	2120.9	40.7(38)	1.69(15)	$13/2^+ \rightarrow 9/2^+$
1438.4	3425.8	1987.4	53.2(25)	1.46(18)	$13/2^- \rightarrow 9/2^-$
1500.8	9104.4	7603.6	2.7(4)	1.57(31)	$27/2^+ \rightarrow 23/2^+$
1538.6	7603.6	6065.0	3.0(4)	1.45(28)	$23/2^+ \rightarrow 19/2^+$
1587.7	6065.0	4476.0	1.9(3)	1.81(28)	$19/2^+ \rightarrow 15/2^+$
1618.3	3425.8	1807.5	11.1(13)	1.45(21)	$13/2^- \rightarrow 9/2^-$
1740.8	1807.5	66.7	24.6(20)	1.79(26)	$9/2^- \rightarrow 5/2^-$
1848.5	5146.1	3297.6	1.0(1)	1.33(27)	$15/2^+ \rightarrow 11/2^+$
1920.2	1987.4	66.7	26.5(26)	1.90(25)	$9/2^- \rightarrow 5/2^-$
2078.2	4205.8	2128.3	1.5(2)	1.19(24)	$13/2^+ \rightarrow 11/2^-$
2085.3	4205.8	2120.9	2.8(4)	1.89(31)	$13/2^+ \rightarrow 9/2^+$

[a]Uncertainties between 0.2 and 0.6 keV.
[b]Doublet: Value given for composite peak.

as $I_\gamma(40^\circ)/I_\gamma(90^\circ)$. The typical ADO ratios for the stretched quadrupole and stretched pure dipole transitions are found to be 1.6 and 0.9, respectively.

III. RESULTS AND DISCUSSION

The partial level scheme of ^{61}Ni deduced from the present work is shown in Fig. 1. It was constructed from the γ-γ coincidence relationships, intensity balances, and ADO ratios. The results are summarized in Table I. The typical γ-ray spectra which support the proposed level scheme are shown in Fig. 2. With five neutrons outside the ^{56}Ni doubly magic core, the low-lying levels in ^{61}Ni are associated with the $p_{3/2}$, $f_{5/2}$, $p_{1/2}$, and $g_{9/2}$ neutron orbitals, and have been observed in many previous experiments [34,38]. The present analyses confirm these levels and support the previous spin-parity assignments.

Based on the ADO ratio analyses and the coincident relationships, a positive-parity dipole band (band 1) and a positive-parity quadrupole band (band 2) at medium-to-high

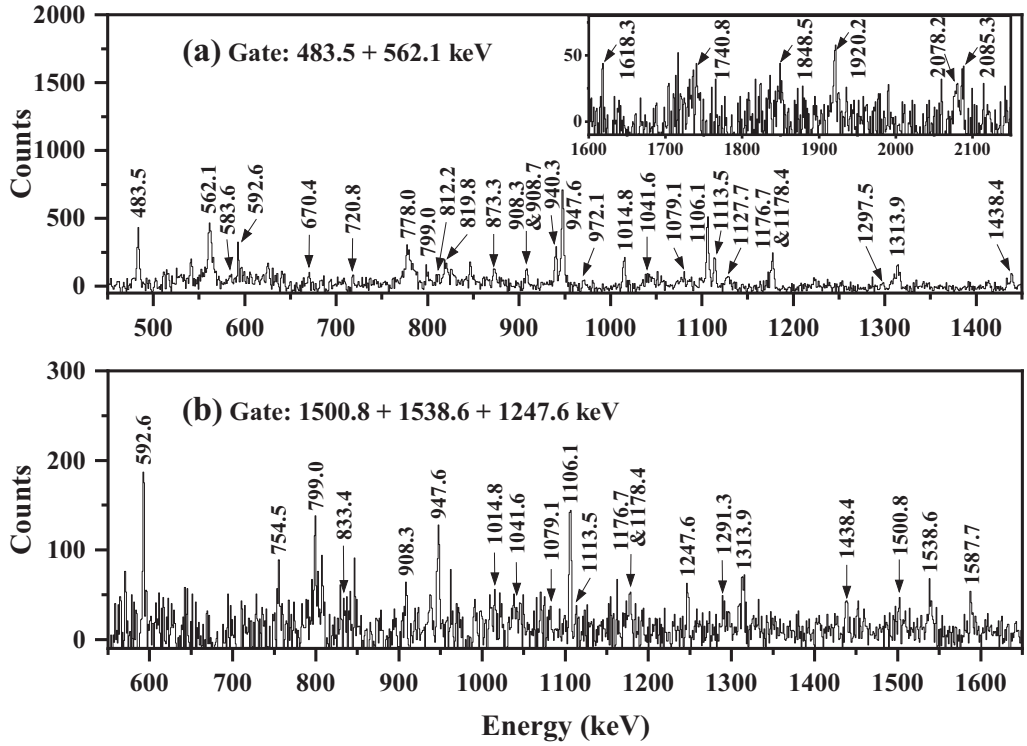

FIG. 2. Coincident spectra for ^{61}Ni, gated on the (a) 483.5 + 562.1 keV transitions, and (b) 1500.8 + 1538.6 + 1247.6 keV.

excitation energies are newly established in the present work. For band 1, a transition cascade of 483.5, 562.1, and 940.3 keV has been reported in Ref. [38] and suggested to have $M1$ characters. In the present work, the dipole characters of 483.5-, 562.1-, and 940.3-keV transitions have been confirmed but their sequences have been modified based on the observation of 670.4-, 812.2-, 1127.7-, and 1848.5-keV cross transitions. In addition, three new $M1$ transitions of 778.0, 819.8, and 873.3 keV are added to the top of band 1 as shown in Fig. 1. In the neighboring isotope ^{60}Ni, four high-lying dipole bands (two negative-parity and two positive-parity) have been observed [33] and interpreted as the MR bands with high-j $1g_{9/2}$ neutron and $1f_{7/2}$ proton-hole configurations involved [33,41]. The similarity between band 1 in ^{61}Ni and the negative-parity MR bands in ^{60}Ni, i.e., M-1 and M-4 bands with the $\pi[(1f_{7/2})^{-1}(fp)^1] \otimes \nu[(1g_{9/2})^1(fp)^3]$ configuration in Ref. [33], indicates that band 1 in ^{61}Ni may also be a MR band with the same high-j configuration but one more neutron in the fp orbital.

For band 2, the $11/2^+$ spin-parity has been assigned to the level at 4476.0 keV based on the $M1 + E2$ character of 1041.6-keV transition to the $13/2^+$ level at 3434.8 keV [38]. Here, although the ADO value of the new 1178.4-keV transition to the $11/2^+$ level at 3297.6 keV could not be extracted, both the dipole characters of the 833.4 keV transition deexcited from the $17/2^+$ level at 5309.7 keV and the 670.4 keV transition deexcited from the $15/2^+$ level at 5146.1 keV to this level, as well as the $M1 + E2$ character of the 1041.6-keV transition, support the $15/2^+$ spin-parity assignment rather than the $11/2^+$ for the level at 4476.0 keV. According to the ADO values obtained in the current work, the quadrupole assignments are made for the three new transitions of 1587.7, 1538.6, and 1500.8 keV.

The high-lying quadrupole band 2 in ^{61}Ni is likely to have the configuration involving multiple $f_{7/2}$ proton holes and $g_{9/2}$ neutrons and is reminiscent of the antimagnetic rotation. To reveal the features of the newly observed collective structures in ^{61}Ni, the I-ω plots for band 1 and band 2 are shown in Fig. 3, in comparison with the well-known MR and AMR bands in ^{110}Cd [4,22,42] and the corresponding $\hat{I}$-$\hat{\omega}$ plot of the classical particles-plus-rotor model. This classical particles-plus-rotor model was devised by Macchiavelli *et al.* to study the competition between the shears mechanism and the core rotation [43], and developed by Sugawara *et al.* to include both magnetic and antimagnetic rotations [30]. In this model, high-j protons and neutrons are represented by classical angular-momentum vectors (blades), and the total energy is expressed as the sum of the rotational energy of the core and effective interactions between the blades in the form $V[(3\cos^2\theta - 1)/2]$ with θ being the shears angle. For simplicity, magnitudes of each proton and neutron vector blade are assumed to be the same. Detailed description of this model can be found in Refs. [30,43]. It can be seen that although this comparison is qualitative, the I-ω features of ^{61}Ni and ^{110}Cd are similar and accord with the predictions of the classical particles-plus-rotor model. Therefore, band 1 and band 2 in ^{61}Ni can be taken as candidates for the MR and AMR bands, respectively.

To further study the properties of band 1 and band 2 in ^{61}Ni, especially their angular-momentum-forming mechanisms, the TAC-CDFT [6,41,44] calculations with the PC-PK1 density functional [45] are performed. Based on the covariant density

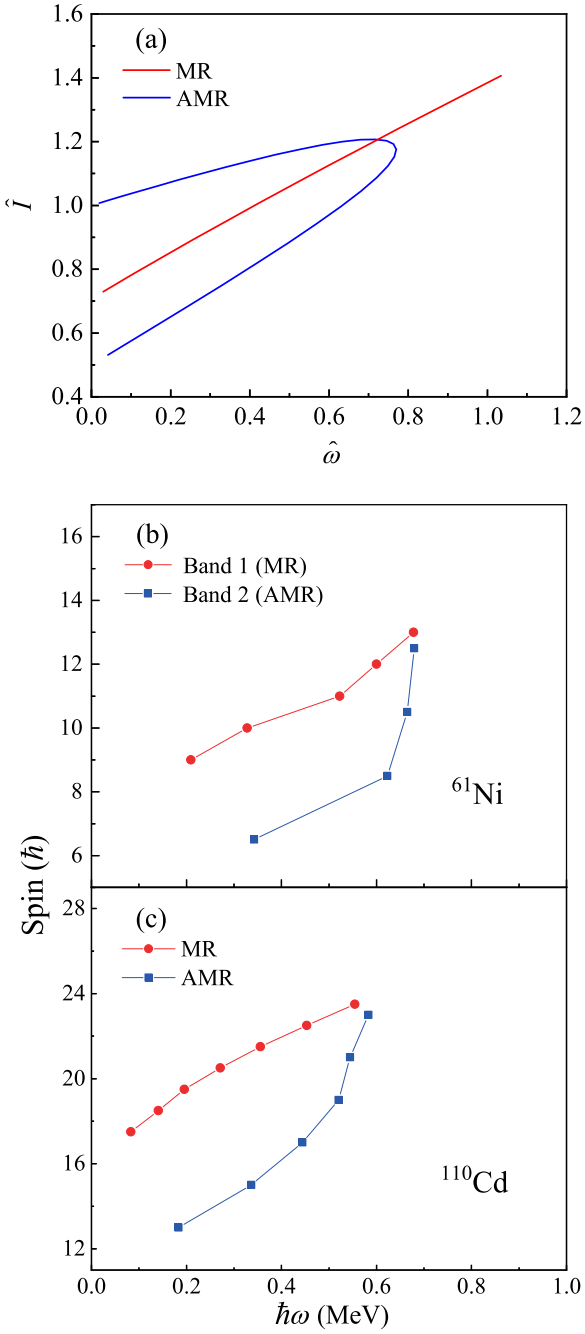

FIG. 3. (a) A typical $\hat{I}$-$\hat{\omega}$ plot of the classical particles-plus-rotor model for MR and AMR. The I-ω plots of (b) the candidate MR and AMR bands in ^{61}Ni, and (c) the well-known MR and AMR bands in ^{110}Cd.

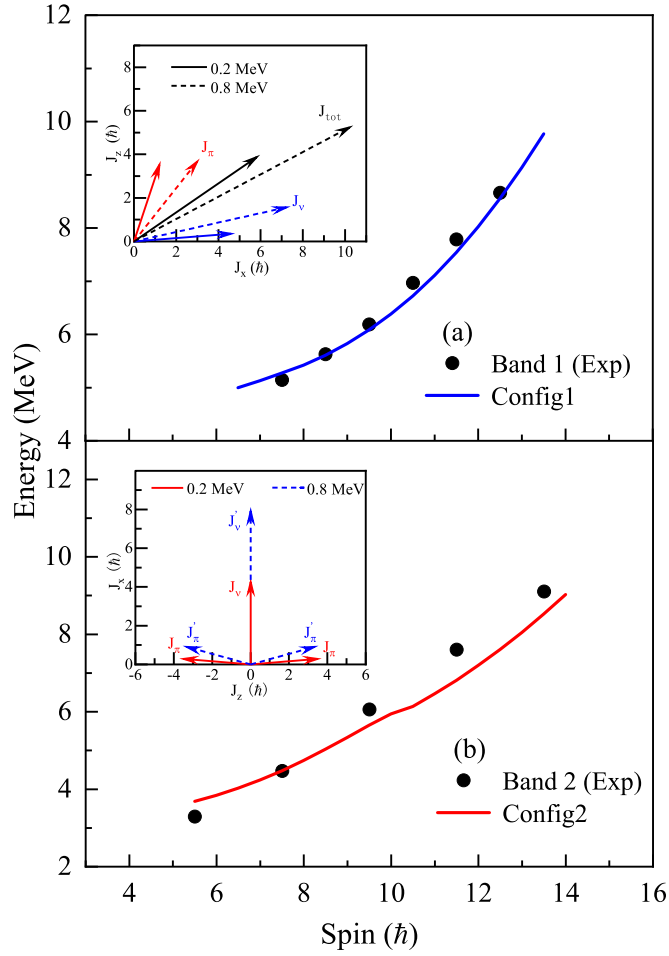

FIG. 4. The calculated energy spectra as functions of spin by TAC-CDFT calculations in comparison with the experimental data for (a) band 1 and (b) band 2 of ^{61}Ni. Insets in panels (a) and (b) show the composition of the proton and neutron angular-momentum vectors $\boldsymbol{J}_\pi$ and $\boldsymbol{J}_\nu$ as well as the total angular-momentum vector $\boldsymbol{J}_{\rm tot} = \boldsymbol{J}_\pi + \boldsymbol{J}_\nu$ at rotational frequencies $\hbar\omega = 0.2$ and 0.8 MeV in TAC-CDFT calculations with Config1 and Config2, respectively.

functional theory [46–49], the tilted axis cranking calculations have been successfully applied to describe many collective structural phenomena, such as magnetic [19,31,41,44] and antimagnetic [31,50,51] rotations, transitions of nuclear spin orientation [52], chiral rotation [53], and rotations with an exotic rod shape [54]. The cranking relativistic Hartree-Bogoliubov equation is solved in the three-dimensional harmonic oscillator bases in Cartesian coordinates with 10 major shells, which provides convergent results for nuclei in the $A \approx 60$ mass region [41]. A finite range separable pairing force [55] is used to consider the pairing correlations, and the scaling factor of the pairing strength is taken from Ref. [56] according to the global analysis of nuclear ground-state properties.

In the present calculations, the valence nucleon configuration of band 1 is $\pi[(1f_{7/2})^{-1}(fp)^1] \otimes \nu[(1g_{9/2})^1(fp)^4]$ and that of band 2 is $\pi[(1f_{7/2})^{-2}(fp)^2] \otimes \nu[(1g_{9/2})^1(fp)^4]$. For convenience, these two configurations are labeled hereafter as Config1 and Config2, respectively. In Fig. 4, the calculated energy spectra as functions of spin are compared with the experimental data. It can be seen that the theoretical calculations reproduce the experimental excitation energies of band 1 and band 2 satisfactorily, which further supports the configuration assignment.

The theoretical transition probabilities $B(M1)$ with Config1 are plotted in Fig. 5. It demonstrates that the TAC-CDFT predicts strong $M1$ transitions for band 1. The $B(M1)$ value is

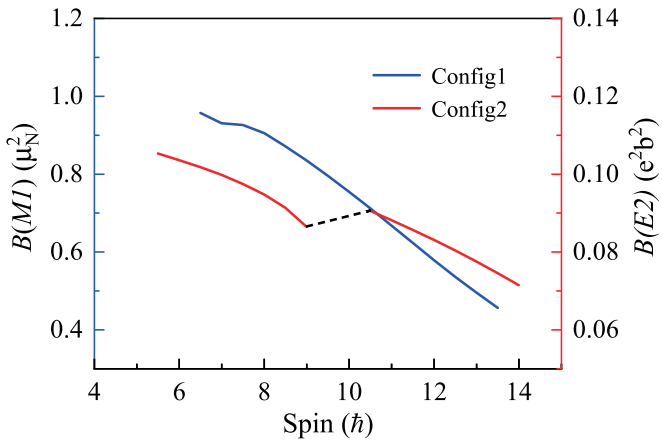

FIG. 5. $B(M1)$ and $B(E2)$ values as functions of spin for band 1 and band 2 of ^{61}Ni by the TAC-CDFT calculations with the assigned configurations.

about $1.0\mu_N^2$ at the bandhead and decreases gradually with the spin, which is consistent with the picture expected for a MR band.

To examine the angular-momentum-forming mechanism of band 1 in ^{61}Ni, the proton and neutron angular-momentum vectors $\boldsymbol{J}_\pi$ and $\boldsymbol{J}_\nu$ as well as the total angular-momentum vector $\boldsymbol{J}_{\rm tot} = \boldsymbol{J}_\pi + \boldsymbol{J}_\nu$ at rotational frequencies $\hbar\omega = 0.2$ and 0.8 MeV are calculated and shown in the inset of Fig. 4(a). In the case of $\hbar\omega = 0.2$ MeV, the proton angular-momentum vector $\boldsymbol{J}_\pi$ comes mainly from the $1f_{7/2}$ hole and aligns closely to the z axis, whereas the neutron angular-momentum vector $\boldsymbol{J}_\nu$ comes mainly from the $1g_{9/2}$ particle and aligns closely to the x-axis. This kind of arrangement of angular momentum leads to a large transverse component of the magnetic-dipole moment and, thus, the enhanced $M1$ transitions [6]. As the increase of rotational frequency, the proton and neutron angular-momentum vectors move toward each other to provide larger total angular momentum, while its direction keeps nearly unchanged. Meanwhile, the closing of proton and neutron angular-momentum vectors reduces the transverse component of the magnetic-dipole moment and therefore, results in smaller $B(M1)$ values.

In contrast with the strong $M1$ transitions observed in the MR band, the AMR band is characterized by weak $E2$ transitions decreasing with spin [4]. The $B(E2)$ values predicted by the TAC-CDFT with Config2 are shown as a function of spin in Fig. 5. It can be seen that the predicted $B(E2)$ values for band 2 are very small ($< 0.11\ e^2b^2$), coinciding with the expectation of an AMR band. Excepting for the discontinuous region with spin $I \approx 10\hbar$, the calculated $B(E2)$ values decrease gradually with spin. The discontinuity around $I \approx 10\hbar$ is caused by the sudden pairing collapse, which comes from the fact that the particle number is not conserved in the present TAC-CDFT calculations with pairing correlations treated by the Bogoliubov transformation. It is expected that the $B(E2)$ values would decrease smoothly with spin after the restoration of particle number by using the projection technique which is, however, beyond the scope of the present investigation.

As mentioned above, for the AMR, its angular momentum is generated by the two-shears-like mechanism [4], i.e., by the simultaneous closing of the angular-momentum vectors of the two valance protons toward the total angular-momentum vector of the neutrons, or vice versa. To illustrate the angular-momentum-forming mechanism of band 2 in ^{61}Ni, the corresponding angular-momentum geometry is shown in the inset of Fig. 4(b). At rotational frequency $\hbar\omega = 0.2$ MeV, the two proton angular-momentum vectors orient opposite to each other and are nearly perpendicular to the vector of neutrons. They form the blades of the two shears. As the increase of rotational frequency, the angular-momentum vectors $\boldsymbol{J}_\pi$ of protons close gradually toward the neutron vector $\boldsymbol{J}_\nu$ while the direction of the total angular momentum keeps unchanged. This corresponds to the closings of two pairs of shears and the two-shears-mechanism can thus be clearly demonstrated. It can be noticed that the angular momentum contributed from the closing of two $f_{7/2}$ proton holes is smaller than that from the neutrons, indicating that the collective rotation of ^{61}Ni also plays an important role in generating the total angular momentum. Therefore, band 2 observed in ^{61}Ni is not pure but highly mixed with the collective rotation, which is different from the ideal AMR bands. Note that such strong mixing between the AMR and the collective rotation has been also shown in ^{100}Pd, as in Ref. [57].

IV. SUMMARY

In summary, the high-spin spectroscopy of ^{61}Ni has been studied by the fusion-evaporation reaction ^{54}Cr(^{11}B, $4n$)^{61}Ni at a beam energy of 54 MeV. One dipole band and one quadrupole band in ^{61}Ni are established for the first time. The I-ω features of the dipole band and quadrupole band are very similar to those of the well-known MR and AMR bands in ^{110}Cd and also accord with the predictions of the classical particles-plus-rotor model. The similarity indicates that band 1 and band 2 in ^{61}Ni can be taken as candidates of MR and AMR bands, respectively. Based on the TAC-CDFT calculations with configurations $\pi[(1f_{7/2})^{-1}(fp)^1] \otimes \nu[(1g_{9/2})^1(fp)^4]$ and $\pi[(1f_{7/2})^{-2}(fp)^2] \otimes \nu[(1g_{9/2})^1(fp)^4]$, band 1 and band 2 in ^{61}Ni are shown to be characterized by the shears mechanism and two-shears-like mechanism, respectively. This study provides evidence for possible coexistence of magnetic and antimagnetic rotations in the $A \approx 60$ mass region. To unambiguously confirm this phenomenon, further experimental investigations such as lifetime measurements are strongly desirable.

ACKNOWLEDGMENTS

This work is supported by the National Key R&D Program of China under Grants No. 2018YFA0404403 and No. 2022YFA1602302, the National Natural Science Foundation of China under Grants No. 12035001, No. 12075006, No. 11675003, No. 11875075, No. 12105004, No. 11975315, No. U2167201, No. U1867210, and No. U1932209. The authors wish to thank Dr. Q. W. Fan for making the target and the staff in the tandem accelerator laboratory at the China Institute of Atomic Energy (CIAE), Beijing.

[1] S. Frauendorf, Nucl. Phys. A **557**, 259 (1993).
[2] S. Frauendorf, J. Meng, and J. Reif, in *Proceedings of the Conference on Physics from Large γ-ray Detector Arrays*, Vol. II of Report LBL35687, edited by M. A. Deleplanque (University of California, Berkeley, 1994).
[3] R. M. Clark and A. O. Macchiavelli, Annu. Rev. Nucl. Part. Sci. **50**, 1 (2000).
[4] S. Frauendorf, Rev. Mod. Phys. **73**, 463 (2001).
[5] H. Hübel, Prog. Part. Nucl. Phys. **54**, 1 (2005).
[6] J. Meng, J. Peng, S. Q. Zhang, and P. W. Zhao, Front. Phys. **8**, 55 (2013).
[7] R. M. Clark, S. J. Asztalos, G. Baldsiefen *et al.*, Phys. Rev. Lett. **78**, 1868 (1997).
[8] S. Frauendorf, in *Proceedings of the Workshop on Gammasphere Physics: Berkeley, CA, 1-2 December, 1995*, edited by M. A. Deleplanque, I. Y. Lee, and A. O. Macchiavelli (World Scientific, Singapore, 1996), p. 272.
[9] C. Majumder, H. P. Sharma, S. S. Tiwary, and S. Chakraborty, Braz. J. Phys. **49**, 539 (2019).
[10] S. Zhu, U. Garg, A. V. Afanasjev *et al.*, Phys. Rev. C **64**, 041302(R) (2001).
[11] M. Sugawara, T. Hayakawa, M. Oshima *et al.*, Phys. Rev. C **92**, 024309 (2015).
[12] N. Rather, S. Roy, P. Datta, S. Chattopadhyay, A. Goswami, S. Nag, R. Palit, S. Pal, S. Saha, J. Sethi, T. Trivedi, and H. C. Jain, Phys. Rev. C **89**, 061303(R) (2014).
[13] S. Sihotra, D. Kumar, M. Kaur, V. Singh, S. Saha, J. Sethi, R. Palit, N. Singh, and D. Mehta, Phys. Rev. C **102**, 034321 (2020).
[14] A. Sharma, R. Raut, S. Muralithar *et al.*, Phys. Rev. C **103**, 024324 (2021).
[15] V. Singh, S. Sihotra, S. Roy *et al.*, J. Phys. G **44**, 075105 (2017).
[16] D. Choudhury, A. K. Jain, M. Patial, N. Gupta, P. Arumugam, A. Dhal, R. K. Sinha, L. Chaturvedi, P. K. Joshi, T. Trivedi, R. Palit, S. Kumar, R. Garg, S. Mandal, D. Negi, G. Mohanto, S. Muralithar, R. P. Singh, N. Madhavan, R. K. Bhowmik, and S. C. Pancholi, Phys. Rev. C **82**, 061308(R) (2010).
[17] A. J. Simons, R. Wadsworth, D. G. Jenkins *et al.*, Phys. Rev. Lett. **91**, 162501 (2003).
[18] D. Choudhury, A. K. Jain, G. A. Kumar *et al.*, Phys. Rev. C **87**, 034304 (2013).
[19] A. J. Simons, R. Wadsworth, D. G. Jenkins *et al.*, Phys. Rev. C **72**, 024318 (2005).
[20] P. Datta, S. Chattopadhyay, S. Bhattacharya, T. K. Ghosh, A. Goswami, S. Pal, M. SahaSarkar, H. C. Jain, P. K. Joshi, R. K. Bhowmik, R. Kumar, N. Madhaban, S. Muralithar, P. V. Rao, and R. P. Singh, Phys. Rev. C **71**, 041305(R) (2005).
[21] C. J. Chiara, S. J. Asztalos, B. Busse *et al.*, Phys. Rev. C **61**, 034318 (2000).
[22] S. Roy, S. Chattopadhyay, P. Datta *et al.*, Phys. Lett. B **694**, 322 (2011).
[23] C. J. Chiara, D. B. Fossan, V. P. Janzen *et al.*, Phys. Rev. C **64**, 054314 (2001).
[24] M. Wang, W. J. Sun, B. H. Sun *et al.*, Eur. Phys. J. A **56**, 31 (2020).
[25] X. W. Li, J. Li, J. B. Lu *et al.*, Phys. Rev. C **86**, 057305 (2012).
[26] K. Y. Ma, J. B. Lu, J. Li *et al.*, Phys. Rev. C **100**, 014326 (2019).
[27] C. M. Petrache, S. Frauendorf, B. F. Lv, A. Astier, E. Dupont, S. Guo, M. L. Liu, X. H. Zhou, K. L. Wang, P. T. Greenlees, H. Badran, D. M. Cox, T. Grahn, R. Julin, S. Juutinen, J. Konki, J. Pakarinen, P. Papadakis, J. Partanen, P. Rahkila, M. Sandzelius, J. Saren, C. Scholey, J. Sorri, S. Stolze, J. Uusitalo, B. Cederwall, O. Aktas, A. Ertoprak, H. Liu, I. Kuti, J. Timar, A. Tucholski, J. Srebrny, and C. Andreoiu, Phys. Rev. C **99**, 041301(R) (2019).
[28] S. Ali, S. Rajbanshi, B. Das, S. Chattopadhyay, M. SahaSarkar, A. Goswami, R. Raut, A. Bisoi, S. Nag, S. Saha, J. Sethi, R. Palit, G. Gangopadhyay, T. Bhattacharjee, S. Bhattacharyya, G. Mukherjee, A. K. Singh, and T. Trivedi, Phys. Rev. C **96**, 021304(R) (2017).
[29] S. Rajbanshi, S. Roy, S. Nag *et al.*, Phys. Lett. B **748**, 387 (2015).
[30] M. Sugawara, Y. Toh, M. Oshima *et al.*, Phys. Rev. C **79**, 064321 (2009).
[31] J. Peng and P. W. Zhao, Phys. Rev. C **91**, 044329 (2015).
[32] D. Steppenbeck, R. V. F. Janssens, S. J. Freeman *et al.*, Phys. Rev. C **85**, 044316 (2012).
[33] D. A. Torres, F. Cristancho, L.-L. Andersson *et al.*, Phys. Rev. C **78**, 054318 (2008).
[34] K. Zuber and B. Singh, Nucl. Data Sheets **125**, 1 (2015).
[35] R. Wadsworth, G. D. Jones, A. Kogan *et al.*, J. Phys. G: Nucl. Phys. **3**, 833 (1977).
[36] R. Wadsworth, A. Kogan, P. R. G. Lornie *et al.*, J. Phys. G: Nucl. Phys. **3**, 35 (1977).
[37] E. K. Warburton, J. W. Olness, A. M. Nathan, and A. R. Poletti, Phys. Rev. C **18**, 1637 (1978).
[38] S. Samanta, S. Das, R. Bhattacharjee *et al.*, Phys. Rev. C **99**, 014315 (2019).
[39] D. Radford, Nucl. Instrum. Methods Phys. Res., Sect. A **361**, 297 (1995).
[40] M. Piiparinen, A. Atac, J. Blomqvist *et al.*, Nucl. Phys. A **605**, 191 (1996).
[41] P. W. Zhao, S. Q. Zhang, J. Peng *et al.*, Phys. Lett. B **699**, 181 (2011).
[42] S. Juutinen, R. Julin, M. Piiparinen *et al.*, Nucl. Phys. A **573**, 306 (1994).
[43] A. Macchiavelli, R. Clark, M. Deleplanque *et al.*, Phys. Lett. B **450**, 1 (1999).
[44] J. Peng, J. Meng, P. Ring, and S. Q. Zhang, Phys. Rev. C **78**, 024313 (2008).
[45] P. W. Zhao, Z. P. Li, J. M. Yao, and J. Meng, Phys. Rev. C **82**, 054319 (2010).
[46] P. Ring, Prog. Part. Nucl. Phys. **37**, 193 (1996).
[47] D. Vretenar, A. Afanasjev, G. Lalazissis, and P. Ring, Phys. Rep. **409**, 101 (2005).
[48] J. Meng, H. Toki, S. Zhou *et al.*, Prog. Part. Nucl. Phys. **57**, 470 (2006).
[49] J. Meng, *Relativistic Density Functional for Nuclear Structure* (World Scientific, Singapore, 2016).
[50] P. W. Zhao, J. Peng, H. Z. Liang *et al.*, Phys. Rev. Lett. **107**, 122501 (2011).
[51] P. W. Zhao, J. Peng, H. Z. Liang *et al.*, Phys. Rev. C **85**, 054310 (2012).
[52] P. W. Zhao, S. Q. Zhang, and J. Meng, Phys. Rev. C **92**, 034319 (2015).
[53] P. Zhao, Phys. Lett. B **773**, 1 (2017).
[54] P. W. Zhao, N. Itagaki, and J. Meng, Phys. Rev. Lett. **115**, 022501 (2015).
[55] Y. Tian, Z. Ma, and P. Ring, Phys. Lett. B **676**, 44 (2009).
[56] S. E. Agbemava, A. V. Afanasjev, D. Ray, and P. Ring, Phys. Rev. C **89**, 054320 (2014).
[57] J. Q. Ma and Z. H. Zhang, Nucl. Phys. A **1016**, 122319 (2021).